ORIGINAL PAPER



Flow structure and rock-breaking feature of the self-rotating nozzle for radial jet drilling

Hua-Lin Liao^{1,2} · Xia Jia^{1,2} · Ji-Lei Niu^{1,2} · Yu-Cai Shi^{1,2} · Hong-Chen Gu³ · Jun-Fu Xu³

Received: 24 September 2018 © The Author(s) 2019

Abstract

For improving the hole-enlarging capability, roundness and rock-breaking efficiency of the nozzle in radial jet drilling, a new structure of self-rotating nozzle was put forward. The flow structure and rock-breaking features of the self-rotating nozzle were investigated with sliding mesh model and labortary tests and also compared with the straight and the swirling integrated nozzle and multi-orifice nozzle which have been applied in radial jet drilling. The results show that the self-rotating jet is energy concentrated, has longer effective distance, better hole-enlarging capability and roundness and impacts larger circular area at the bottom of the drilling hole, compared with the other two nozzles. Forward jet flow generated from the nozzle is peak shaped, and the jet velocity attenuates slowly at the outer edge. Due to periodic rotary percussion, the pressure fluctuates periodically on rock surface, improving shear and tensile failures on the rock matrix and thereby enhancing rock-breaking efficiency. The numerical simulation results of the flow structure of the nozzle are consistent with the experiments. This study provides an innovative approach for radial jet drilling technology in the petroleum industry.

Keywords Self-rotating nozzle · Flow field characteristic · Numerical simulation · Rock-breaking

1 Introduction

Radial jet drilling (RJD) is a process of drilling radial horizontal holes of small diameter using high-pressure water jets (Dickinson et al. 1992a, b, 1993; Landers 1998). The milling bit makes a turn of 90 degrees to create a hole in a cased wellbore and subsequently to jet a small hole into the formation through the casing exit hole. The diameter of these radial holes is approximately 1–2 inches, and lengths

Edited by Yan-Hua Sun

- Yu-Cai Shi shiyucai2008@163.com

Published online: 09 November 2019

- Key Laboratory of Unconventional Oil and Gas Development (China University of Petroleum (East China)), Ministry of Education, Qingdao 266580, Shandong, China
- School of Petroleum Engineering, China University of Petroleum (East China), Qingdao 266580, Shandong, China
- ³ Shengli Offshore Drilling Co, SINOPEC, Dongying 257000, Shandong, China

are up to 300 ft as shown in Fig. 1 (Dickinson et al. 1992a, b; Buckman and Doton 2001; Kamel 2016). It can realize multiple radial holes drilling in different directions in a reservoir, increase the contact area between reservoir and bore hole, enhance well production rate, and has been widely applied or tested in low-permeability reservoirs, marginal reservoirs, depleted reservoirs, heavy-oil reservoirs, fault block reservoirs and coalbed methane (CBM) reservoirs in the USA, Canada, China, Egypt, Argentina, India and Russia, among other countries (Buset et al. 2001; Cirigliano and Blacutt 2007; Bruni et al. 2007; Ursegov et al. 2008; Huang et al. 2013; Steven and Ahmed 2013; Balch et al. 2016). A high-pressure flexible hose is employed to realize the right diversion in the casing deflector and convey water-jet energy to break the rock (Wang et al. 2016; Kamel 2017; Yang et al. 2015). The nozzle used in RJD is important since it provides pulling force for flexible hose as well as breaks rock in front of it to form a horizontal hole. The jet penetrating features in different rocks along with various nozzle configurations are important to RJD. Engineering practice shows that the hole-enlarging capability and rock-breaking efficiency of the nozzle have become main problems to be solved (Buckman and Doton 2003; Putra et al. 2012). Some nozzles cannot drill to objective depths due to irregular outline of hole and



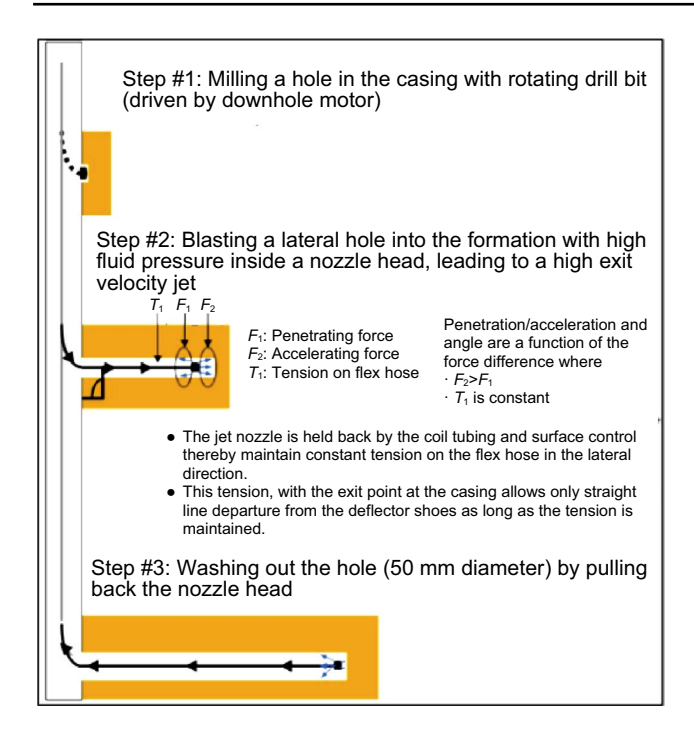


Fig. 1 RJD process (Courtesy of RadJet)

excess friction of flexible hose. Hence, as a key component in RJD, the performance of the nozzle directly influences rock-breaking effect and extending length of RJD. Currently, the multi-orifice nozzle (Liao et al. 2011; Li et al. 2015), the swirling nozzle and the straight and swirling integrated nozzle have been applied in RJD (Liao et al. 2013a, b; Chi et al. 2016). The swirling nozzle has larger impacting area and better diffusivity, but the velocity attenuates faster. If the rock strength or confining pressure is relatively high, the rock-breaking efficiency and hole-enlarging capability will be limited. The multi-orifice nozzle is jet energy concentrated with a better rock-breaking efficiency, but the number of orifices distributed in the nozzle limits the hole roundness. Straight and swirling integrated nozzle incorporates

both advantages of the straight and swirling jets, but the jet energy utilization is relatively lower as well as the rock-breaking efficiency. This study designed a new structure of self-rotating nozzle and conducted both numerical simulations of flow features and rock-breaking tests to quantify adaptabilities in RJD with various nozzle configurations.

2 Self-rotating nozzle structure and its working principle

As shown in Fig. 2, a self-rotating nozzle consists of a rotator, a rotating shaft, a shell, a rotary clearance seal, and forward and backward orifices. Forward and backward orifices are both installed on the rotator, and the forward and backward jets are formed as fluids are ejected from these forward and backward orifices in the rotator. Since the axis of backward orifices has a certain offset from the axis of rotation, backward jets can generate rotating torque accordingly, making the rotator to overcome frictional force and driving the forward and backward orifices to rotate around the nozzle axis. As the rotator keeps rotating, multiple forward jets form several concentric ring impact faces on the rock surface and further develop to form a complete circular impact area to break the rock. This will help to improve the hole roundness and rock-breaking efficiency. Simultaneously, by optimizing the angle of forward orifices, the hole-enlarging capability of the nozzle will be effectively enhanced. The axial reverse thrust from backward orifices is larger than that from forward orifices, and thus a pulling force is imposed to move the facilitate hose along the drilling direction. This makes the nozzle capable of pulling the flexible hose, realizing breaking rock while rotating and self-propelling. The rotary clearance seal allows a small amount of water leakage through the spiral groove on the outer-wall of the rotating shaft, and therefore the rotational friction of the shaft can be reduced.

The rotational speed of the rotator is calculated from the pressure fluctuation caused by periodic impact of the jet under rotational conditions, which is measured with the

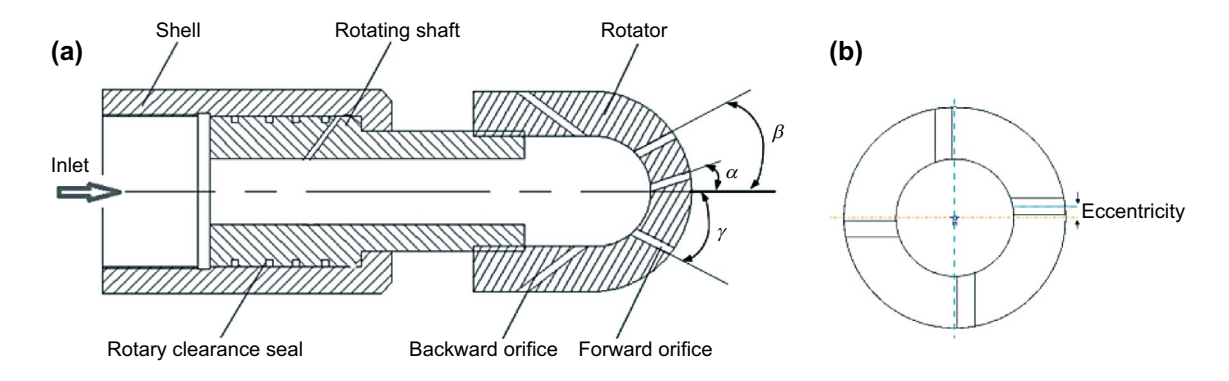


Fig. 2 Schematic diagram of the self-rotating nozzle. a Structure. b Eccentric structure of backward orifices



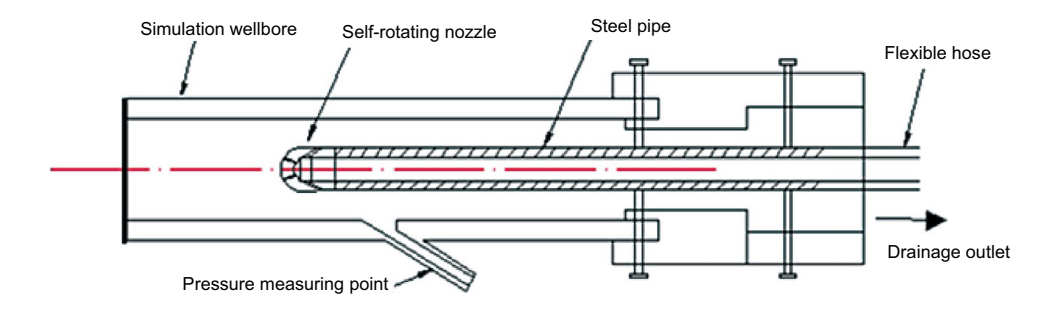
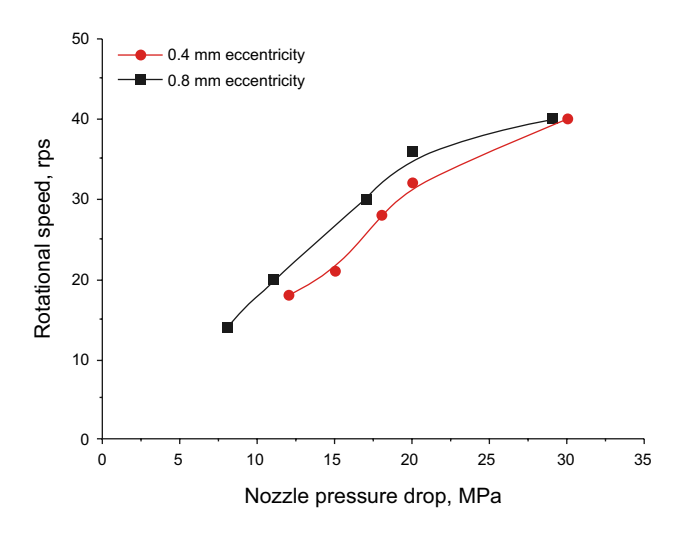


Fig. 3 A device for measuring the rotational speed of the rotator



 $\label{fig.4} \textbf{Fig. 4} \ \ \textbf{The relationship between the rotational speed and the nozzle pressure drop}$

device shown in Fig. 3. Figure 4 shows the influence of the nozzle pressure drop on the rotational speed of the nozzle rotor. The rotational speed of the rotator increases, but the increasing rate slows down with an increase in the nozzle pressure drop. For instance, the rotational speed of the rotor changes from 17.5 to 40.0 revolutions per second (rps) when the nozzle pressure drop increases from 10 to 30 MPa.

3 Numerical model and boundary conditions

3.1 Simulation model

To optimize the numerical simulation, the physical model is simplified. Only computational domain within the rotator is kept for the self-rotating nozzle, while the effect of fluid flow in the rotating axis of the nozzle is not considered. Figure 5 shows a three-dimensional physical model of the rotator, and Fig. 6 shows a physical model of bottom hole for the nozzle.

The outer diameter of the nozzle rotator is 18 mm, with a length of 30 mm. The leading end surface of the rotator



Fig. 5 Three-dimensional physical model of the nozzle rotator

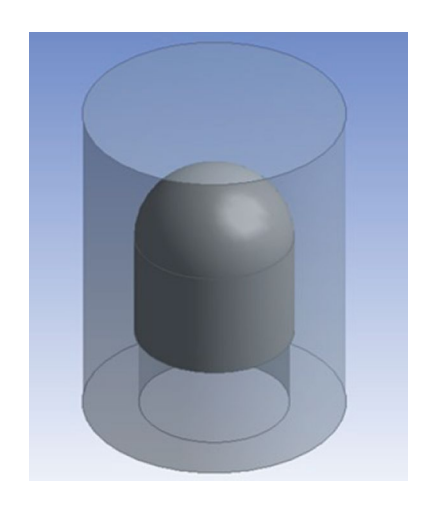


Fig. 6 A physical model of the bottom hole for the nozzle

is round, and the main inner flow diameter is 3 mm. There are 3 forward orifices and 4 backward orifices on the rotator. The forward orifices have the same diameter of 0.8 mm, with the intersection angles α , β , γ of their axes to the nozzle axis being 7°, 13° and 20°, respectively. Backward orifices also have the same diameter of 1.2 mm, with the same 30° intersection angles of their axes to the nozzle axis, and each



has an eccentricity of 0.8 mm. The leading end of the nozzle is 10 mm away from the bottom of the outer flow field. The horizontal cross section of the outer flow field is circular, 14 mm in radius and 50 mm in height.

3.2 Mesh of computational domain

ICEM-CFD software was used to build the sliding mesh model, and the flow structure of the nozzle under a steady rotational state is simulated as shown in Fig. 7, in which the computational domain is separated into two sections, namely the rotator and the stator, respectively. In the numerical calculation, a rotating velocity is set up by the rotator to simulate the flow field structure of the nozzle when it rotates. The unstructured mesh generation method is adopted in the computational domain, and the mesh refinement measures are taken for the parts where the velocity gradient changes sharply to ensure the stability of the computational process and the correctness of the computational results. There are more than 2.3 million mesh in the whole computational domain.

3.3 Control equations

In numerical simulations, the RNG k– ε turbulence model was used to obtain a detailed visual flow field structure of the rotating jet. The set of equations of the model is similar to that of the standard k– ε model, but with an additional R in the transmission equation of ε . Thus, the model can more accurately describe swirling and impinging jet flows (Chen et al. 2003; Anderson et al. 2009). Buoyancy forces are not taken into account for incompressible fluids. The control equations in the RNG k– ε model mainly include continuity and momentum equations as well as transmission equations of the turbulent kinetic energy k and the dissipation rate ε .

(1) Continuity equation

$$\frac{\partial \rho}{\partial t} + \frac{\partial \rho u_i}{\partial x_i} = 0 \tag{1}$$

(2) Momentum equation

$$\rho \frac{\partial u_i}{\partial t} + \rho u_j \frac{\partial u_i}{\partial x_j} = -\frac{\partial \overline{p}}{\partial x_i} + \frac{\partial}{\partial x_j} \\ \left[\left(\mu_0 + \mu_t \right) \left(\frac{\partial u_i}{\partial x_j} + \frac{\partial u_j}{\partial x_i} \right) - \frac{2}{3} \left(\rho k + \mu_t \frac{\partial u_i}{\partial x_i} \right) \delta_{ij} \right]$$
(2)

(3) Transmission equations

$$\frac{\partial(\rho k)}{\partial t} + \frac{\partial(\rho u_i k)}{\partial x_i} = \frac{\partial}{\partial x_i} \left(\alpha_k \left(\mu_0 + \mu_t \right) \frac{\partial k}{\partial x_i} \right) + \mu_t S^2 - \rho \varepsilon$$
(3)

$$\begin{split} \frac{\partial(\rho\varepsilon)}{\partial t} + \frac{\partial(\rho u_i \varepsilon)}{\partial x_i} &= \frac{\partial}{\partial x_i} \left(\alpha_{\varepsilon} \left(\mu_0 + \mu_{t} \right) \frac{\partial \varepsilon}{\partial x_i} \right) \\ &+ C_{1\varepsilon} \frac{\varepsilon}{k} \mu_{t} S^2 - C_{2\varepsilon} \rho \frac{\varepsilon^2}{k} - R \end{split} \tag{4}$$

$$S = \sqrt{2S_{ij}S_{ij}}, S_{ij} = \frac{1}{2} \left(\frac{\partial u_j}{\partial x_i} + \frac{\partial u_i}{\partial x_j} \right)$$

$$R = \frac{C_{\mu}\rho\eta^{3}(1 - \eta/\eta_{0})}{1 + \beta\eta^{3}} \frac{\varepsilon^{2}}{k}$$

where ρ is the fluid density; t is time; $\overline{\rho}$ is pressure; u_i , u_j (i, j=1, 2, 3) represent the velocity; x_i , x_j represent coordinate axis; δ_{ij} is Kronecker symbol; μ_0 is the fluid viscosity; μ_t represents the turbulence viscosity, $\mu_t = \rho C_{\mu} k^2 / \varepsilon$; C_{μ} , $C_{1\varepsilon}$, $C_{2\varepsilon}$ are empirical coefficients

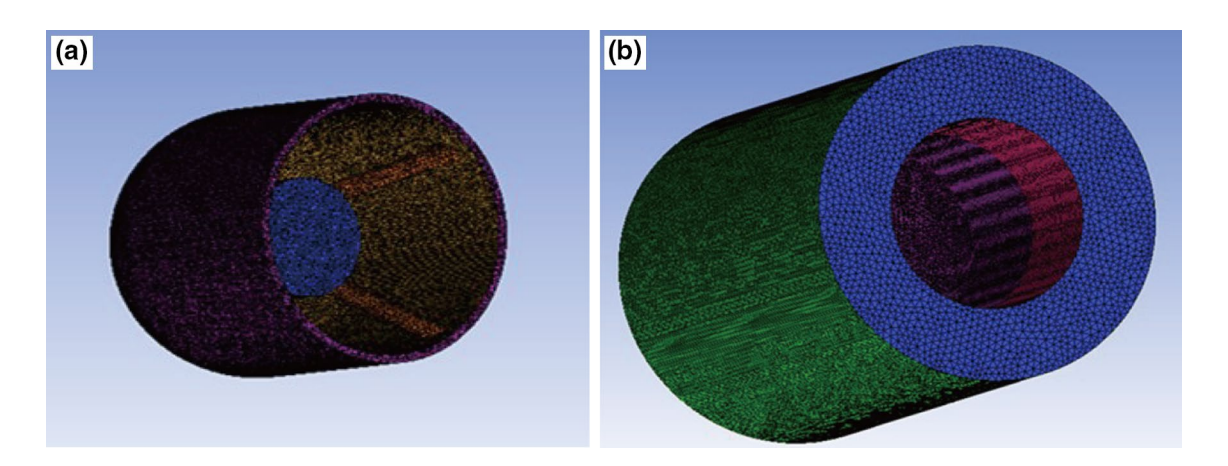


Fig. 7 3D mesh model of numerical simulation. a Rotator. b Stator



set to 0.09, 1.42, 1.68, respectively, in the model; $\alpha_k = \alpha_{\varepsilon} \approx 1.393; \eta \equiv Sk/\varepsilon, \beta = 0.012.$

R is the difference between the RNG $k-\varepsilon$ model and the standard $k-\varepsilon$ model. The existence of R enables the RNG $k-\varepsilon$ model to simulate flow with high strain and allows the flow lines to be more accurately depicted.

Solutions to the discretized equation were reached using the tridiagonal matrix algorithm (TDMA), in which the low relaxation iteration was done line by line. The coupled and iterative solution for continuity and momentum equations were worked out using the SIMPLEC algorithm.

3.4 Parameters and boundary conditions

As the nozzle rotator has a high rotational velocity, the RNG k– ε model was adopted, which has a higher accuracy for flow fields with high flow curvature and strain rate (Song et al. 2004, 2017). At the same time, a SIMPLE algorithm was used to solve the continuity equations and momentum equations with coupling iteration. The rotational speed of the rotator is set to 0, 25, 50 and 75 rps to be discussed later and the test results are shown in Fig. 4.

Boundary conditions are set as follows:

(1) Inlet boundary The inlet velocity depends on inlet conditions in which k and ε are computed from the equations below:

$$I = 0.16(Re)^{1/8} \tag{5}$$

$$k = 1.5 \left(v_{\rm in} I \right)^2 \tag{6}$$

$$\varepsilon = C_{\mu}^{0.75} k^{1.5} / (0.07 L_{\rm in})$$
 (7)

where Re is the Reynolds number; $v_{\rm in}$ is the inlet velocity; I is the turbulent intensity; $L_{\rm in}$ is the length of the mixing section at the inlet.

- (2) *Outlet boundary* The static pressure for the outlet is set to 0.1 MPa.
- (3) Wall boundary conditions The relative angular velocity at the rotator wall boundary is set to zero. Non-slip boundary condition is applied to other walls.

$$U_{+p} = \frac{1}{\kappa} \ln \left(E y_{+p} \right) \tag{8}$$

$$y_{+p} = \frac{C_{\mu}^{1/4} k_p^{1/2} y_p}{p} \tag{9}$$

where U_{+p} is the dimensionless velocity of point p near the wall; κ is the Karman constant, $\kappa = 0.4$; E is the

wall roughness for the hydraulically smooth surface E = 9.0; y_p is the distance computed from point p to the wall; v is the kinematic viscosity. To guarantee the applicability of the law of logarithmic distribution for velocity, the value of y_{+p} is set in the range as:

$$11.5 \sim 30 \le y_{+p} \le 200 \sim 400$$

4 Results and discussion

4.1 Distribution and variation trend of the jet impact zone

Figure 8 shows flow field distributions of forward jets at the bottom of the hole at different durations. It reflects the distribution of forward jet impact area while the rotor is rotating. As shown, there is basically no variation of the single jet impact area. Three forward jets form almost three circular impact areas at the bottom of the hole, and each jet moves around the center of the impact circle, forming a complete circular impact surface. Compared with the multi-orifice jet flow field, the self-rotating nozzle with fewer forward orifices can generate a larger impact area and guarantee hole roundness when their equivalent diameters are the same.

Figure 9 shows the simulated pressure fluctuation of a certain point at the bottom of the hole. It can be seen that when jets rotate, a periodic fluctuation of pressure is formed on the rock surface. The rotating jets impact periodically on the rock surface, generating shear and tensile failures at every point and contributing to a higher rock-breaking efficiency (Shen 1998; Bu et al. 2003).

4.2 Flow characteristics of forward jets

4.2.1 Axial velocity attenuation

Figure 10 shows the attenuation of the axial velocity of the jets from forward orifices. The Y-axis is the normalized axial velocity $v/v_{\rm max}$ (v is the axial velocity of the jet; $v_{\rm max}$ is the maximum axial velocity of the jet), and X-axis is the normalized jetting distance D/d (D is the jetting distance; d is the equivalent diameter of forward orifices). A larger jet angle of forward orifices forms a larger rotational radius at the bottom of the hole; as a result, the jetting distance decreases. It can be seen that when forward jets eject from orifices, the axial velocities of jets rapidly attenuate as the normalized jetting distance increases, and the velocities reduce to 0 at the boundary wall. Furthermore, the axial velocity of the 20° jet is lower than that of the other two jets, which means the larger the jet angle, the more the jet velocity attenuates. Near the boundary wall, three jetting velocities gradually



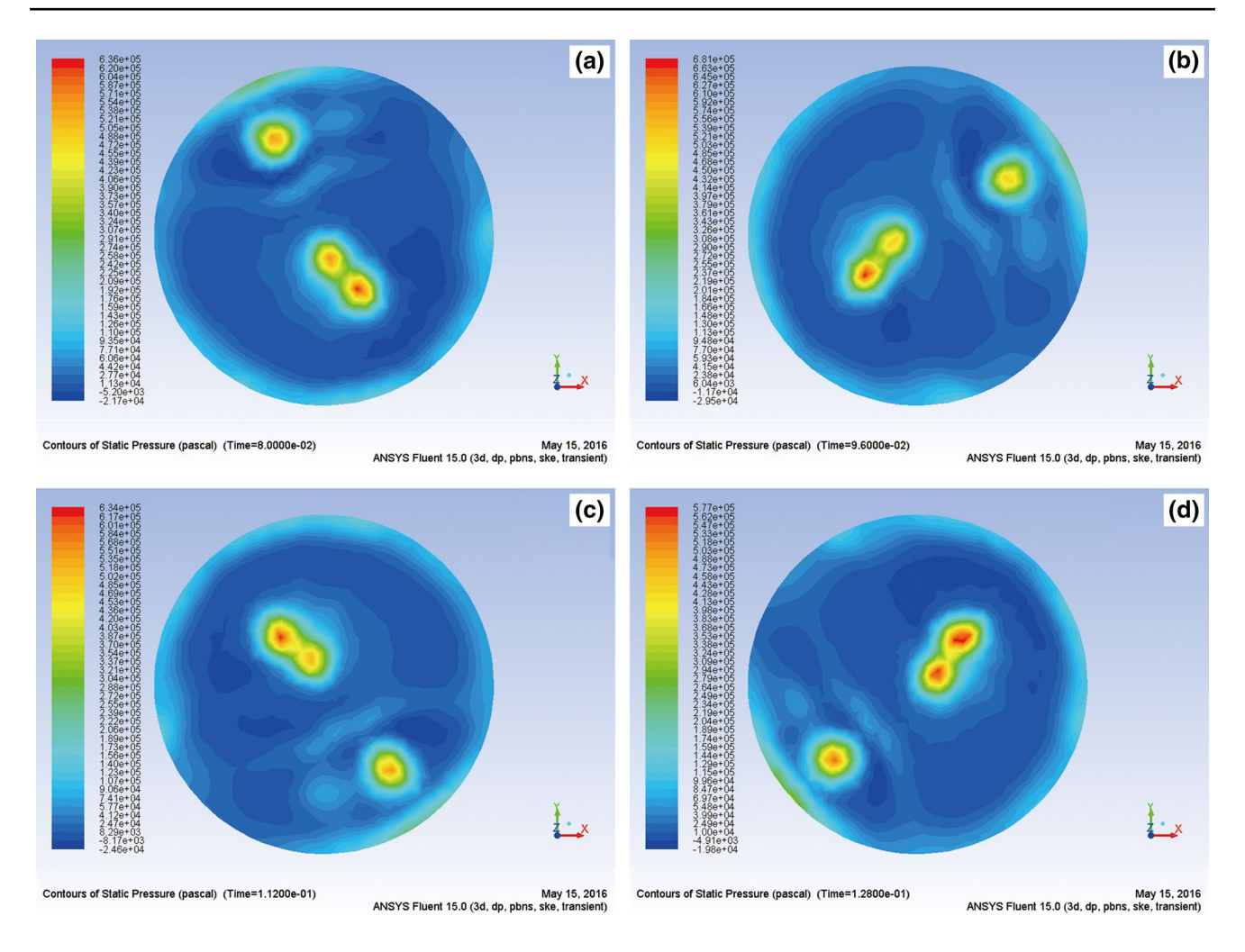


Fig. 8 Distribution of flow field at the bottom of the hole at different durations. a 0.080 s. b 0.096 s. c 0.112 s. d 0.128 s

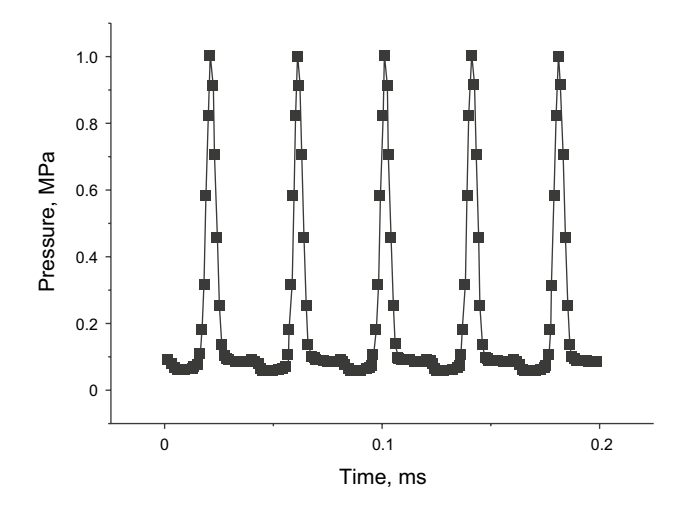


Fig. 9 Pressure fluctuation at the bottom of the hole

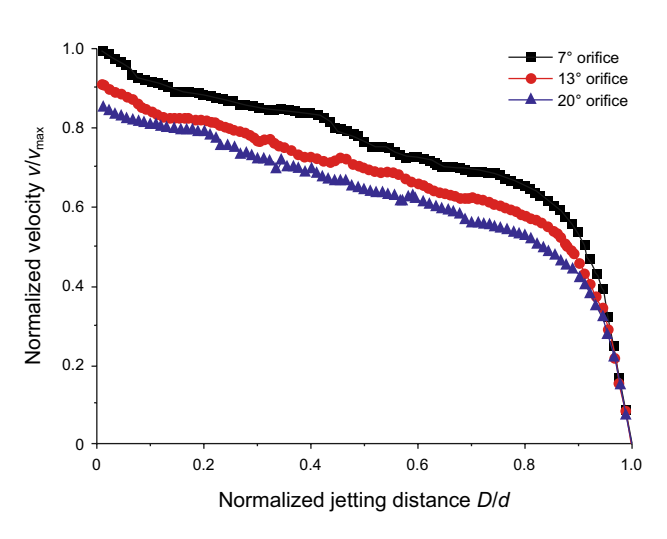


Fig. 10 Attenuation of the axial velocity of jets ejected from different forward orifices



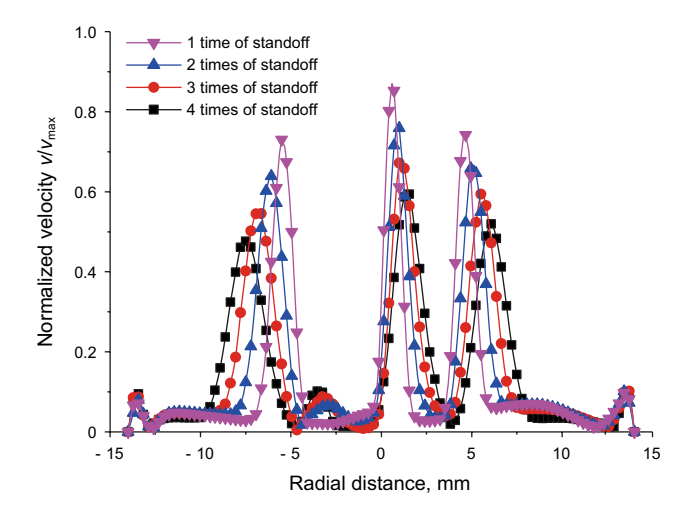


Fig. 11 Distribution of axial velocities at different standoff distances

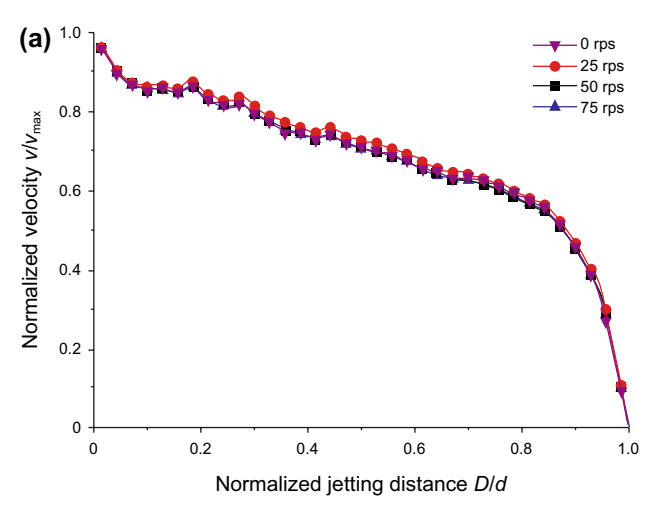
become similar. It is concluded that the larger the jet angle is, the greater the influence of the wall effect on the jet, and the faster the attenuation of the axial velocity is.

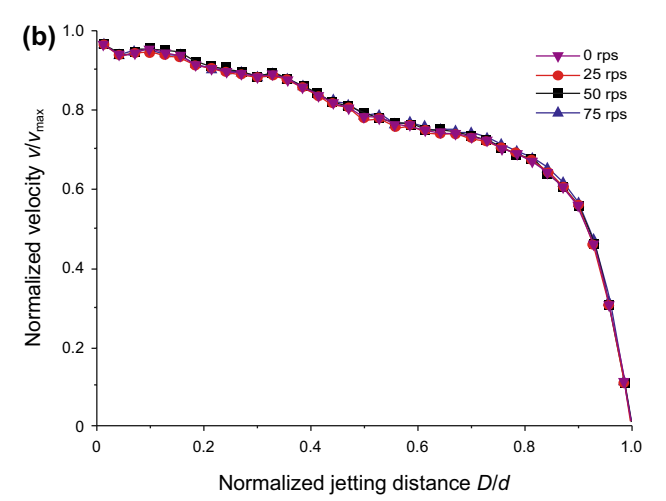
4.2.2 Axial velocity distribution

Figure 11 gives the distribution of the axial velocity of the forward jet at different standoff distances. It can be seen that the normalized velocity in the whole cross section is peak-shaped at different standoff distances. Each peak corresponds to a forward orifice, and there is a low velocity zone between two peaks. Because of jetting angles of forward orifices, the peaks move away from the impact center as the standoff distance increases. Also, increasing standoff distances will decrease the axial velocities but gradually increase the impact area. It can also be inferred with an increase in standoff distance, the impact area increases and the hole diameter drilled by the jet will be enlarged accordingly.

4.3 Impact of rotational speed of rotor on flow characteristics

Figure 12 shows velocity attenuations along forward orifice axes at different rotational speeds. As can be seen, the impact of rotation on the attenuation of jet velocities from orifices increases with the intersection angles α , β , γ . The axial velocity attenuation of jet with 20° intersection angle is obviously affected by the rotational speeds set from 0 to 75 rps. The rock-breaking depth is mainly influenced by jet velocity and its erosion duration. Since the orifice with 20° intersection angle has less acting time on the rock and the velocity attenuates faster, it yields shallower breaking





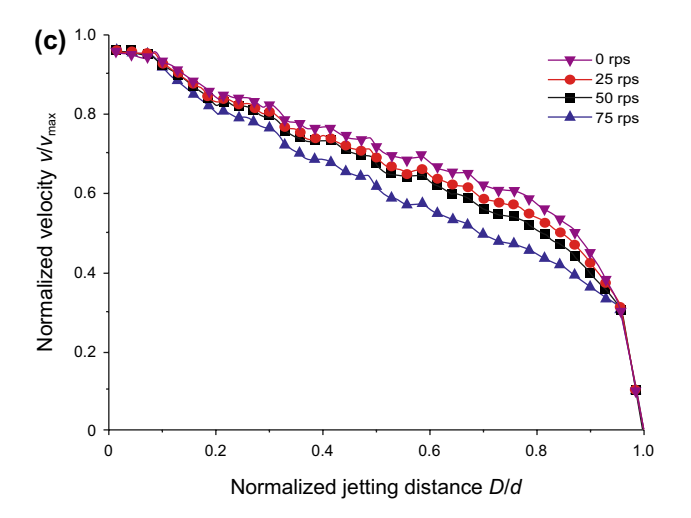
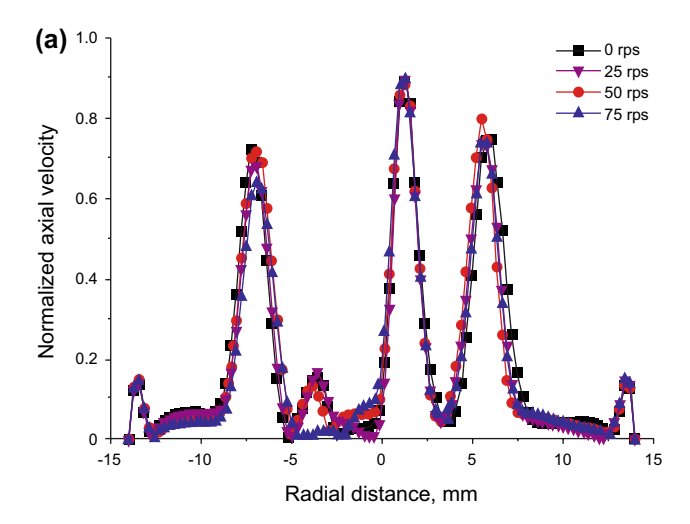
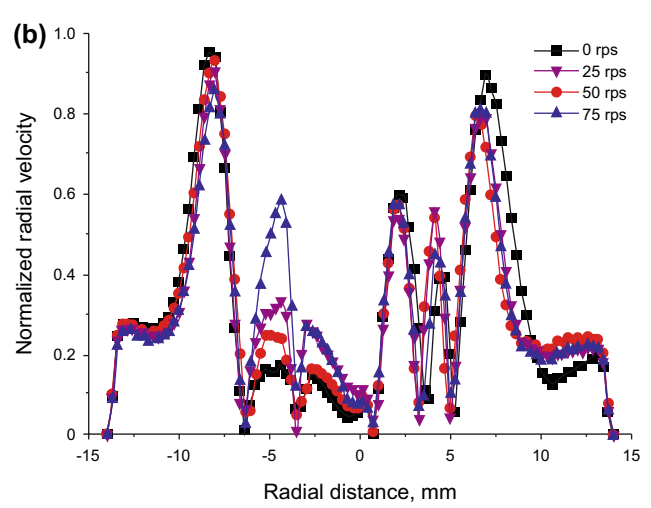


Fig. 12 Axial velocity attenuation along forward orifice axes. a 7° orifice. b 13° orifice. c 20° orifice

depth compared with multi-orifice and straight and swirling integrated nozzles illustrated in later rock test, and a T-type crater is formed at the bottom of the hole.







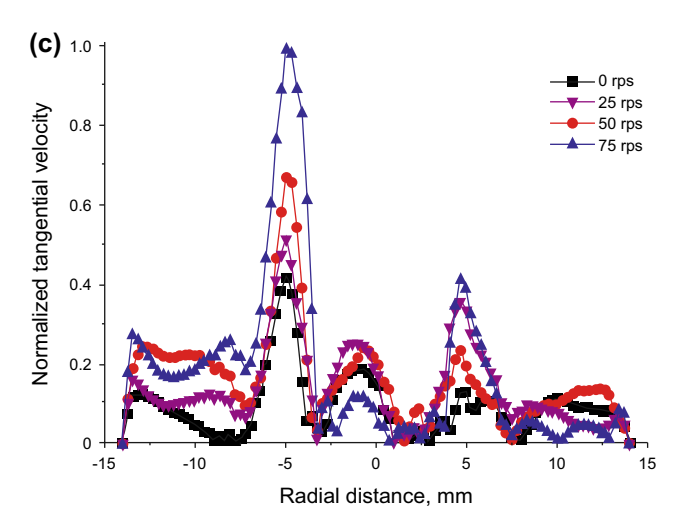


Fig. 13 Velocity distributions of forward jets at different rotational speeds. a Axial velocity. b Radial velocity. c Tangential velocity

Figure 13 shows the velocity distribution of forward jets at the bottom of the hole at different rotational speeds; from the figure, the following inference could be obtained:

- (1) The axial velocity of the forward jet at different rotational speeds presents a peak distribution at the bottom of the hole. The maximum values of the three peaks are basically the same, and the size of the velocity distribution area is basically unchanged. The axial velocity distribution is basically independent on the rotational speed.
- (2) Under different rotational speeds, the radial velocity of the three forward jets corresponds to the bottom hole position with three peaks, and the peak value is basically the same. There are "peaks" with smaller peaks among the three peaks. The analysis shows that the distance between the three jets is small, and the diffuse flow produced by the two forward jets is mutually contradictory and strengthened, thus forming a radial velocity concentrated zone.
- (3) The tangential velocity of forward jets with different intersection angles corresponds to three peaks in the figure. The tangential velocity of jet with 20° intersection angle is the highest, followed by the 13° angle, and the lowest is the 7° angle. With an increase in rotational speed, the peak of the tangential velocity of forward jet increases. From the mechanism of rock fragmentation, it can be seen that the high tangential velocity of jet is helpful to the tensile and shear failure of rock and to reduce the threshold pressure of rock breakage (Shen 1998).

Through numerical simulation of the flow structure of self-rotating jets, flow structure, it is found that forward orifices including angles α , β , γ have an important influence on jet flow characteristics. Four groups of nozzles were manufactured with the configurations of forward orifice with intersection angles $\alpha-\beta-\gamma$ set as $7^{\circ}-13^{\circ}-20^{\circ}$, $7^{\circ}-12^{\circ}-20^{\circ}$, $7^{\circ}-11^{\circ}-18^{\circ}$ and $7^{\circ}-11^{\circ}-20^{\circ}$. In order to make the rotor rotate smoothly, the centerlines of the forward orifices and the rotor are kept in the same planes, whereas the axes of two backward orifices offset from the axes of the rotor by 0.4 mm, and the equivalent diameter of all forward orifices is 2 mm.

Figure 14 shows the rock-breaking features with the above nozzles under a pressure drop of 30 MPa, a dimensionless standoff distance of 3 times, and an erosion time of 4 min. It can be seen that the self-rotating nozzles can drill round holes with clear outline. Among them, the hole drilled by the nozzle with the intersection angle of 7°–13°–20° is more rounded and regular as shown in Fig. 14a, while there are obvious central holes in the center of the holes by other structural configurations as illustrated in Fig. 14b–d.

To evaluate the rock-breaking performance of the self-rotating nozzle, comparative rock-breaking tests were conducted using the multi-orifice nozzle and the straight and swirling integrated nozzle illustrated in Fig. 15 which have been widely applied in industry. Figure 16 shows a



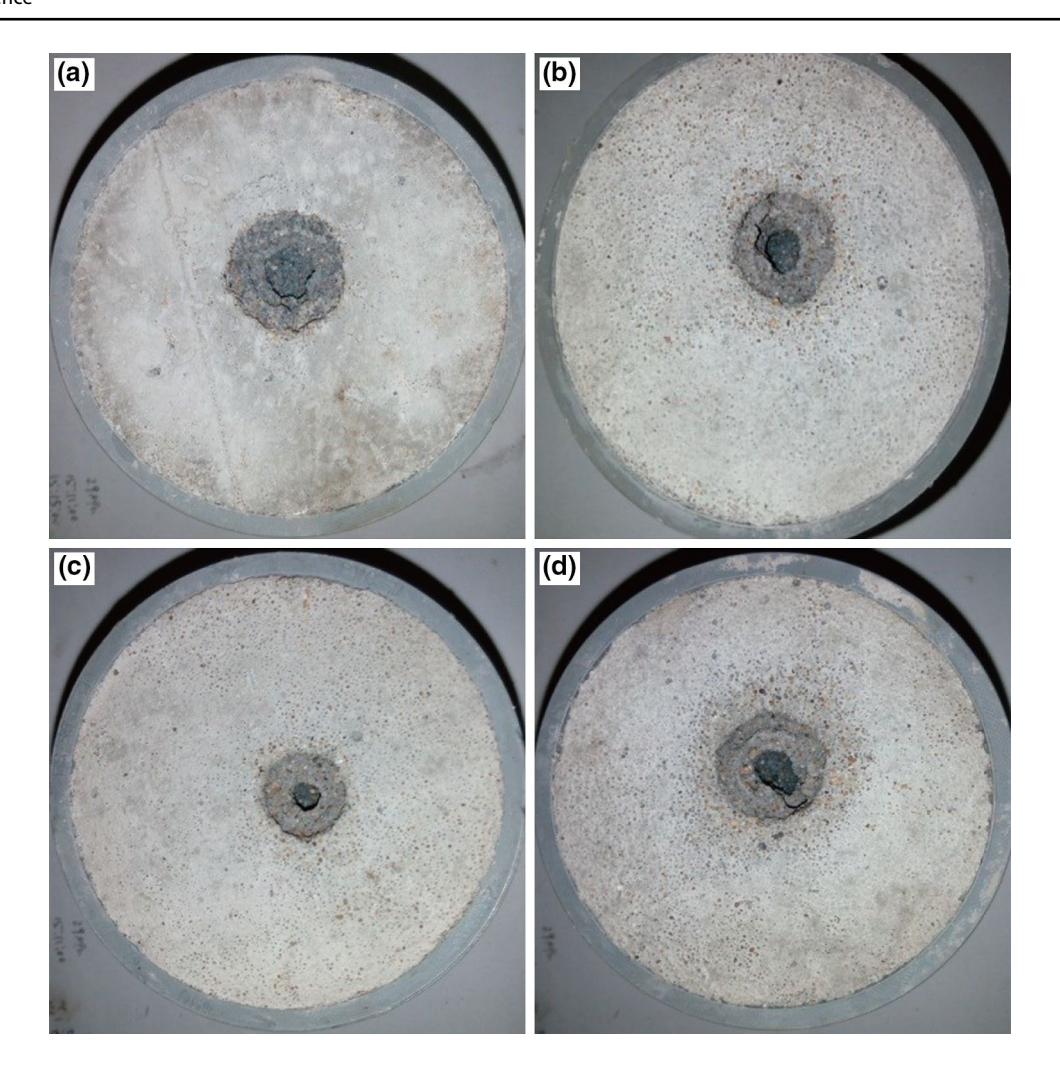


Fig. 14 Holes drilled using nozzles with various angles of $\alpha-\beta-\gamma$. a $7^{\circ}-13^{\circ}-20^{\circ}$. b $7^{\circ}-12^{\circ}-20^{\circ}$. c $7^{\circ}-11^{\circ}-18^{\circ}$. d $7^{\circ}-11^{\circ}-20^{\circ}$

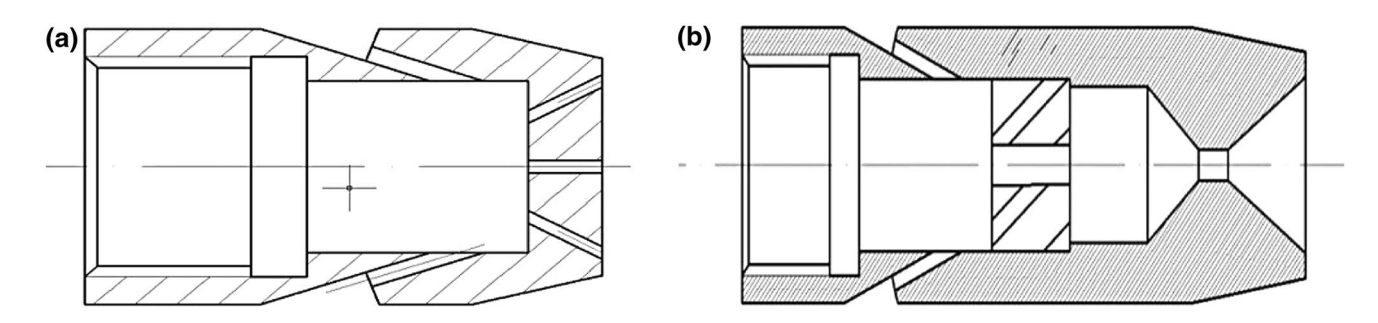


Fig. 15 Schematic diagrams of other two nozzles. a Multi-orifice nozzle. b Straight and swirling integrated nozzle

comparison of rock-breaking characteristics of the three nozzles which have the same equivalent diameter forward orifices and backward orifices under the conditions of pressure drop of 30 MPa, 3 times of dimensionless standoff distance and erosion time of 4 min. It can be seen that the hole generated by the self-rotating nozzle is round, the hole outline is clear, and the borehole diameter is larger. In the contrast, the outer edge of the hole drilled by the multi-orifice nozzle is plum-shaped and irregular, with a roughly similar depth as well as that drilled by the self-rotating nozzle. While the hole drilled by the straight and swirling integrated nozzle is nearly circular, its roundness and depth is less than that drilled by the self-rotating nozzle. Also, the outer edge is



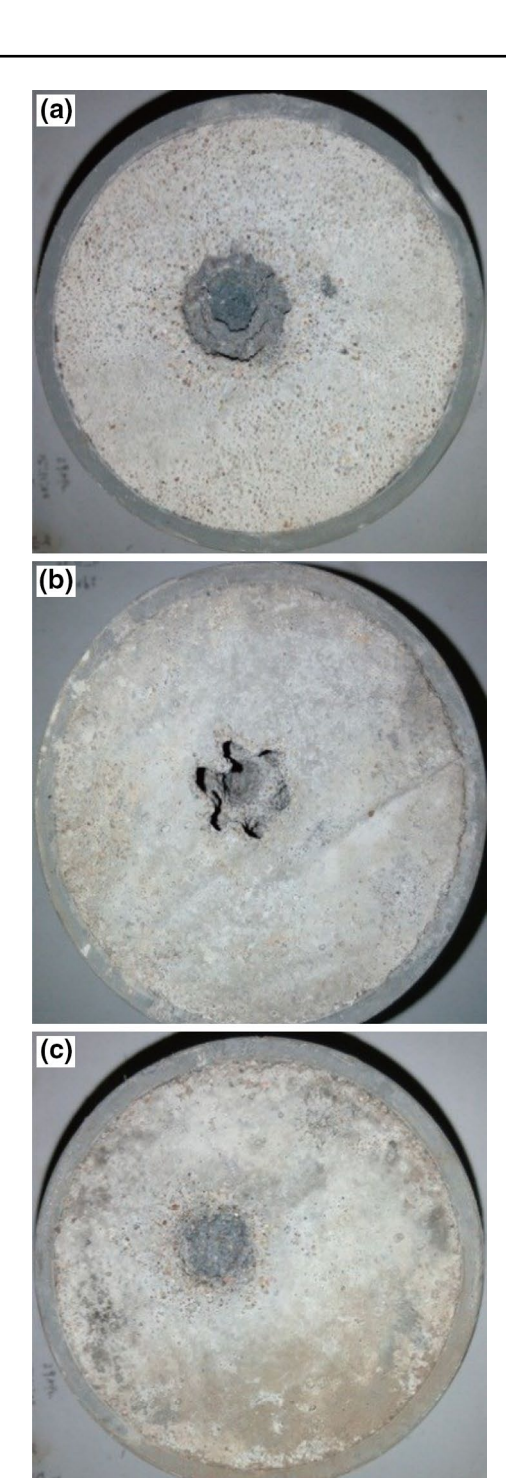


Fig. 16 Features of holes drilled by a self-rotating nozzle, b multi-orifice nozzle, c straight and swirling integrated nozzle

unclear, and the hole diameter is larger than that drilled by the multi-orifice nozzle, but the crater is shallower.

Combining numerical simulations and the rock-breaking tests, the self-rotating nozzle shows the similar axial velocity attenuation in comparison with the multi-orifice nozzle, and thus it can achieve desirable rock-breaking depth. At

the same time, because of the rotating impact mode of the self-rotating nozzle, a circular impact surface is formed at the bottom of the hole, so the impact breakage makes the drilling hole more smooth and round which is a benefit for reducing friction during hose movement and reaching longer radial distance. Furthermore, compared with the straight and swirling integrated nozzle, the self-rotating nozzle has an better energy concentrated jet flow core, longer effective jetting distance, and faster radial and tangential velocities; thus, rock can be effectively eroded, and the hole profile is much clearer. Therefore, different types of nozzles generate different types of jets and form various impact patterns on a rock. The multi-orifice jet is energy concentrated, longer in effective jetting distance but limited in impact area; the straight and swirling integrated jet has three-dimensional velocity, more diffusivity, but faster velocity attenuation and shorter effective operating range, resulting in a shallow hole in the rock. The self-rotating jet is energy concentrated and longer in effective jetting range; compared with the other two nozzles, it has stronger reaming capability as well as good drilling roundness, which are exactly what RJD requires.

5 Conclusions

In this paper, a new type of self-rotating nozzle was put forward in order to achieve a longer and rounder hole in radial jet drilling. From the numerical simulation and the rock-breaking test, the nozzle is energy concentrated and has a long effective jetting distance like a multi-orifice nozzle, whereas its three-dimensional velocities are like the straight and swirling integrated nozzle. Therefore, it can drill a rounder and larger hole as compared with the other two nozzles. Simulation reveals that the forward jet flow feature of the self-rotating nozzle has three peak points, among which the outer velocity attenuates slower. Compared with the straight and swirling integrated jet, it can guarantee more effective central erosion and breakage of the outer edge and generate periodic pressure fluctuation on the rock surface, which has the characteristic of pulse jets and assists to improve rock penetration. The tangential velocity of forward jets of the self-rotating nozzle increases as the rotational speed goes up, which enhances shear and tensile failure and achieves a higher rock-breaking efficiency.

The self-rotating nozzle has a potential application, and a number of factors like the nozzle structure and working parameters affect the rock-breaking efficiency. Therefore, more rock-breaking tests need to be conducted for optimizing the nozzle design and work parameters.

Acknowledgements The authors express their appreciation to the supports from Natural Science Foundation of China (Grant No.



51274235), Shandong Provincial Natural Science Foundation (Grant No. ZR2019MEE120) and the Major project of CNPC (Grant No. ZD2019-183-005).

Open Access This article is distributed under the terms of the Creative Commons Attribution 4.0 International License (http://creativecommons.org/licenses/by/4.0/), which permits unrestricted use, distribution, and reproduction in any medium, provided you give appropriate credit to the original author(s) and the source, provide a link to the Creative Commons license, and indicate if changes were made.

References

- Anderson JD, Degroote J, Degrez G, et al. Computational fluid dynamics. Berlin: Springer; 2009.
- Balch RS, Ruan TJ, Savage M, et al. Field testing and validation of a mechanical alternative to radial jet drilling for improving recovery in mature oil wells. In: Western regional meeting, Anchorage, Alaska, USA; 2016. https://doi.org/10.2118/180410-MS.
- Bruni M, Biassotti H, Salomone G. Radial drilling in Argentina. In: Latin American & caribbean petroleum engineering conference, Buenos Aires, Argentina; 2007. https://doi.org/10.2118/10738 2-MS.
- Bu YH, Wang RH, Zhou WD. Study on rock drilling by swirling jet. Chin J Rock Mech Eng. 2003;22(4):664–8 (in Chinese).
- Buckman WG, Doton TL. Method and apparatus for jet drilling drainholes from wells. US patent No. 6263984B1; 2001.
- Buckman WG, Doton TL. Nozzle for jet drilling and associated method. US Patent No. 6668948B2; 2003.
- Buset P, Riiber M, Eek A. Jet drilling tool: cost-effective lateral drilling technology for enhanced oil recovery. In: SPE/ICOTA coiled tubing roundtable, Texas, Houston, USA; 2001. https://doi.org/10.2118/68504-MS.
- Chen QG, Xu Z, Zhang YJ. Application of two versions of a RNG based *k*–*ε* model to numerical simulation of turbulent impinging jet flow. J Hydrodyn (Ser. B). 2003;2(2):71–6.
- Chi HP, Li GS, Liao HL, et al. Effect of parameters of self-propelled multi-orifice nozzle on drilling capability of water jet drilling technology. Int J Rock Mech Min. 2016;86:23–8. https://doi.org/10.1016/j.jipmms.2016.03.017.
- Cirigliano RA, Blacutt JFT. First experience in the application of radial perforation technology in deep wells. In: Latin American & caribbean petroleum engineering conference, Buenos Aires, Argentina; 2007. https://doi.org/10.2118/107182-MS.
- Dickinson W, Dickinson R, Herrera A. Slim hole multiple radial drilled with coiled tubing. In: SPE Latin America petroleum engineering conference, Caracas, Venezuela; 1992a. https://doi.org/10.2118/23639-MS.
- Dickinson W, Dykstra H, Nees JM, et al. The ultrashort radius radial system applied to thermal recovery of heavy oil. In: SPE western regional meeting, Bakersfield, California; 1992b. https://doi.org/10.2118/24087-MS.
- Dickinson W, Dykstra H, Nordlund R. Coiled tubing radials placed by water-jet drilling: field result, theory, and practice. In: 68th Annual technical conference and exhibition of SPE, Texas, Houston, USA; 1993. https://doi.org/10.2118/26348-MS.
- Huang ZW, Li GS, Tang ZJ, et al. Technology of hydra-jet sidetracking of horizontal micro-radial laterals. Pet Drill Tech.

- 2013;41(4):37–41. https://doi.org/10.3969/j.issn.1001-0890.2013.04.009 (in Chinese).
- Kamel AH. Radial jet drilling: a technical review. In: SPE middle east oil & gas show and conference, Manama, Kingdom of Bahrain; 2017. https://doi.org/10.2118/183740-MS.
- Kamel AH. RJD: a cost effective frackless solution for production enhancement in marginal field. In: SPE eastern regional meeting held in Canton, Ohio, USA; 2016. https://doi.org/10.2118/18405 3-MS
- Landers CW. Method of and apparatus for horizontal well drilling. US patent No. 5853056; 1998.
- Li JB, Li GS, Huang ZW, et al. The self-propelled force model of a multi-orifice nozzle for radial jet drilling. J Nat Gas Sci Eng. 2015;24:441–8. https://doi.org/10.1016/j.jngse.2015.04.009.
- Liao HL, Niu JL, Chen YX. Experiment study on water jet breaking rock by multi-orifice nozzle. J China Coal Soc. 2011;36(11):1858– 62. https://doi.org/10.13225/j.cnki.jccs.2011.11.004 (in Chinese).
- Liao HL, Li GS, Niu JL, et al. Integrating straight and swirling jets bit design and it's rock breaking characteristics for radial horizontal hole drilling. J China Coal Soc. 2013a;38(3):424–9. https://doi.org/10.13225/j.cnki.jccs.2013.03.005 (in Chinese).
- Liao HL, Wu DS, Wang L, et al. Comparisons of spraying structure and rock breakage characteristics of round straight jet, swirling jet and straight-swirling integrated jet. Atom Spray. 2013b;23(4):363–77. https://doi.org/10.1615/AtomizSpr.2013007261.
- Putra SK, Sinaga SZ, Marbun BTH. Review of ultrashort-radius radial system (URRS). In: International petroleum technology conference, Bangkok, Thailand; 2012. https://doi.org/10.2523/IPTC-14823-MS.
- Shen ZH. Theory and technology of water jet. Dongying: China University of Petroleum Press; 1998 (in Chinese).
- Song J, Li GS, Hu YT. Numerical simulation of dual jet turbulent flow with combined coaxial swirling and round jet. J Hydrodyn (Ser. A). 2004;19(5):671–5. https://doi.org/10.16076/j.cnki.cjhd.2004.05.017 (in Chinese).
- Song XZ, Liu ZH, Li GS, et al. Numerical analysis of the impact flow field of multi-orifice nozzle hydrothermal jet combined with cooling water. Int J Heat Mass Trans. 2017;114:578–89. https://doi.org/10.1016/j.ijheatmasstransfer.2017.06.106.
- Steven DC, Ahmed HK. Novel technique to drill horizontal laterals revitalizes aging field. In: SPE/IADC Drilling Conference, Amsterdam, The Netherlands; 2013. https://doi.org/10.2118/163405-MS.
- Ursegov S, Bazylev A, Taraskin E. First results of cyclic steam stimulations of vertical wells with radial horizontal bores in heavy oil carbonates. In: SPE Russian oil and gas technical conference and exhibition. Moscow, Russia; 2008. https://doi.org/10.2118/115125-RU.
- Wang B, Li GS, Huang ZW, et al. Lab testing and finite element method simulation of hole deflector performance for radial jet drilling. J Energy Resour-ASME. 2016;139:1–10. https://doi.org/10.1115/1.4035552.
- Yang RY, Huang ZW, Li GS, et al. Slotted liner sheathing coiled tubing-a new concept for multilateral jetting in coalbed methane wells and laboratory tests of tubular friction performance. J Nat Gas Sci Eng. 2015;26:1332–43. https://doi.org/10.1016/j.jngse .2015.08.031.

